

Coherence between superconducting edge states in superconducting periodic arrays of artificial defects

C.C. Abilio¹, L. Amico^{2,4}, Rosario Fazio^{2,3}, and B. Pannetier¹

¹*CNRS-CRTBT, Laboratoire associé à l'Université Joseph Fourier,
25 Av. des Martyrs, 38042 Grenoble Cedex, France*

²*Dip. di Metodologie Fisiche e Chimiche (DMFCI), Università di Catania,
viale A. Doria, I95219 Catania, Italy*

³*Istituto Nazionale di Fisica della Materia (INFM),criteria Unità di Catania*

⁴*Dpto de Fisica Teorica de la Materia Condensada,
Universidad Autonoma de Madrid, Madrid E-28049, Spain.*

The transition line of superconducting arrays of holes exhibits a rich field structure due to the interference of superconducting states nucleated at the holes edges. We studied by means of resistance measurements their effect on the $T_c^(H)$ line as a function of transverse magnetic field using regular arrays of nanofabricated micron size holes. The arrays transition fields are higher than for the bulk. Moreover we found a nontrivial field modulation of the $T_c^*(H)$ line with an inversion, with increasing field, of the modulation concavity which we assigned to a crossover from a collective to an isolated edge state regime. The high field regime is well described by the nucleation at a single hole in an infinite film. The modulation at low fields was found to be dominated by the interference of neighbor edge states when the inter-hole distance w becomes comparable to the coherence length $\xi(T_c^*)$. A comparison between arrays of different hole shape shows the influence of geometry on the type of interaction established, which can be described either as a superconducting wire network or as a weak link array.*

PACS numbers: 74.76.-w, 74.60.Ge, 74.25.Dw

1. Introduction

The effect of artificial pinning centers on the vortex dynamics of type-*II* superconductors has attracted a great interest in both fields of high T_c and conventional low T_c superconductors. The increase interest on low T_c materials is mainly due to the development of nanofabrication techniques which enable the introduction, in a controlled way, of nanoscale defects with a well defined shape and separation distance. These patterned samples constitute relatively simple systems for the study of how artificial defect structures influence vortex dynamics.

Previous experiments on regular superconducting arrays of holes have put in evidence the influence of artificial voids on the array transition line¹. For arrays of sufficiently separated holes the transition line is dominated by the surface edge states nucleated around holes boundaries. Since edge states nucleate at fields H_{c3}^* higher than for nucleation in the bulk H_{c2} , the arrays transition fields are higher than H_{c2} . In addition, the array transition temperature $T_c^*(H)$ presents a rich field modulation due to the phase coherence of the edge states imposed by the external magnetic field over the geometrical lengths of the problem: the hole surface and the elementary cell of the array lattice.

On the other hand, since the edge states localize around the hole on a surface sheath of thickness of the order of $\xi(T)$, the superconducting coherence length, they act as barriers against the entry and exit of magnetic flux from the hole. They dominate the vortex dynamics of the array at temperatures close to $T_c^*(H)$, where the intrinsic pinning is washed out by thermal excitations as has been studied previously^{2,3}.

In this work we shall consider regular arrays in the regime of intermediate hole separation, where the inter-hole distance w ($w > \xi(0)$) becomes comparable to $\xi(T_c^*)$ at low fields, allowing a coupling between neighbor edge states.

The two limit cases, the isolated hole in an infinite superconductor film and the superconducting wire network^{4,5} (vanishing hole separation) are quite well known. In the single hole case, $T_c^*(H)$ depends exclusively on the magnetic flux threading the hole, exhibiting a field modulation characterized by downward oscillations with periodic dips occurring near half integers of the flux quantum $\Phi_o = hc/2e$ per hole⁶. A similar result was found for superconducting disks⁷. In the case of the superconducting wire network, $T_c^*(H)$ is characterized by upward oscillations with a field periodicity of one Φ_o per array elementary cell.

In arrays of intermediate hole separation we can tune a crossover from the isolated hole regime to a regime of coupled edge states by decreasing

the applied field. The relevant parameters for the problem are the external field, $\xi(T_c^*)$ and the array parameters: hole size and lattice constant a . We will try to put forward the role of these parameters on the crossover between these two regimes and how they influence the type of interaction established at low fields.

In the next section we present experimental results obtained for a superconducting square array of holes where the aspect ratio defect size/lattice parameter is approximately 2. These results are compared with those obtained previously ¹ on a different array of similar aspect hole/lattice parameter but with twice the distance between hole edges.

For both samples we identified a clear crossover from single to collective edge state regime in decreasing field. However at low fields we found a different behavior between arrays. This differences are related with the occurrence of distinct nucleation processes, controlled by the ratio w/ξ .

In section 3.2 we analyze the case where the inter-hole distance w is such that at low fields $w/\xi(T_c^*)$ is lower than the critical ratio 1.84 ⁸. The low field nucleation is then dominated by thin wire superconducting edge states and the coupling is well described by the formalism of superconducting wire networks ^{4,5}.

In section 3.3 we analyze the case $w/\xi(T_c^*) > 1.84$ where edge nucleation is determined by a single boundary condition at the holes edges but w is still small enough to allow a weak overlap between neighbor edge state wave functions. In this regime the low field behavior can be described using a model based on the presence of a weak link interaction between adjacent edge states. This simple model is able to capture the essential features of the crossover discovered previously ¹.

2. Experimental Details

The array sample consists of a thin film of aluminum (80nm) patterned with a regular square array of nanofabricated holes. The lattice spacing is $4.0\mu m$ and holes have a square shape with $1.85 \pm 0.01\mu m$ side length, the distance between neighbor hole edges being $w = 2.15 \pm 0.01\mu m$ as determined by SEM microscopy. We shall refer to this sample as sample A. The full array size is $1 \times 1 cm^2$ corresponding to a total of 6.25×10^6 holes.

The patterning was defined on a monolayer PMMA coated Si wafer by Deep UV photolithography using a chromium mask. The sample is then prepared using conventional *lift-off* techniques after thermal evaporation of pure aluminum over the resist mask on a UHV chamber. An homogeneous thin film of aluminum evaporated at the same time and submitted to the

same fabrication steps is also measured for a reference of the patterning process effect on the material parameters.

Both samples were studied by conventional four-probe resistance measurements using an AC four terminal resistance bridge at a $33Hz$ frequency and a measuring current of $2nA$. Assuming an uniform current distribution over the array, the current density per wire is $4.5 \times 10^{-4} Acm^{-2}$. The voltage contacts are placed at a distance of $2.8mm$ from each other in the array center to avoid short circuits from the sample borders.

The field dependence of the nucleation temperatures $T_c^*(H)$ is determined using a heating feedback technique that keeps the sample resistance at a constant value while the magnetic induction field is smoothly varied by small increments of $0.2\mu T$. Several resistance criteria between 0.01 and $0.4R_n$ were used. This method enables us to attain a fine field tuning of the array transition line.

Resistance measurements as a function of temperature were also performed at several magnetic fields between 0 and $5mT$, after zero field cooling from a temperature well above T_{co} . The nucleation temperatures determined from $R(T)$ measurements agree by less than $1mK$ with those obtained by the sweeping field method for the same resistance criteria, indicating a good temperature regulation attained by the feedback method.

From the zero field $R(T)$ measurement we can estimate several material parameters. Using a 2D Aslamazov-Larkin fit ⁹, we estimate a BCS transition temperature $T_{co} = 1.262K$ and a normal state resistance of $R_n = 0.099\Omega$. The resistance per single wire of length $a = 4.0\mu m$ and width $w = 2.15\mu m$ is then $r_n = 0.354\Omega$ and the normal state resistivity $\rho_n = 1.49\mu\Omega cm$. Using $v_F = 2.03 \times 10^8 cm/s$ we obtain an electronic mean free path $l_{el} = 26.5nm$. The zero field transition temperature defined at half of the normal state resistance are $1.263K$ and $1.265K$ for the patterned sample and the homogeneous thin film, respectively, the transition width being $3mK$ for both samples. We summarize on Table 1 some parameters of array A and the parameters of the sample previously studied ¹, array B. Array B consists on an aluminum thin film ($80nm$ thickness) patterned with a square array of circular holes of diameter $2r = 4.26\mu m$ and a lattice parameter of $9.0\mu m$.

The transition temperature $T_c^*(H)$ of array A as a function of the applied field is shown in Fig. 1.a). For comparison we show the bulk transition line reconstructed from $H_{c2}(T^*/T_{co}) = (1 - T^*/T_{co})\Phi_0/2\pi\xi^2(0)$, using the reference film coherence length at $T = 0K$, $\xi(0) = 220nm$ (determined from the initial linear slope of the reference film transition line).

We can distinguish a non-trivial field modulation of $T_c^*(H)$: at fields below $0.75mT$ it is characterized by periodic upward cusps which evolve,

Sample	hole shape	a (μm)	w (μm)	T_{co} [K]	$\xi(0)$ (μm)
array A	square	4.0	2.15	1.263	0.25
array B	circle	9.0	4.74	1.25	0.25

Table 1. Some parameters of array A and array B. a is the array lattice constant and w the minimum distance between boundaries of neighbor holes.

at higher fields, into downward dips of larger magnetic period. These field modulations were found independently of the criteria used in the transition line measurement. The crossover between these two field regimes is clearly identified on Fig. 1.b) where the sawtooth variation of the transition line slope $dT_c^*(H)/dH$, at low field gives place to a smoother variation at higher fields, along with the change of magnetic period.

At low fields the magnetic period of $H = 0.128 mT$, corresponding to one Φ_o enclosed on a square cell of side length $a = 4.0 \mu m$, indicates the presence of phase coherence over the array lattice. The larger period oscillations are a reminiscence of the Little and Parks effect ¹⁰, where the quantization of the magnetic flux enclosed on a hollow cylinder determines a field oscillating transition line with downward dips occurring at half integers of Φ_o . In the hole case the magnetic period is not a constant since it depends on the effective surface formed by the hole radius and the surface superconducting sheath surrounding the hole. The average magnetic period is $0.543 mT$ which corresponds to an effective square of side length $l_{hole} = 1.94 \mu m$. The array hole size is $1.85 \mu m$.

3. Discussion

3.1. Extraction of the energies for nucleation of superconductivity

To better understand the field behavior of the nucleation processes involved we shall treat the problem in terms of the energies for nucleation of superconductivity at a given field, ϵ_{nucl} .

The energy ϵ_{nucl} can be obtained by finding the lowest eigenvalue solution of the linear Ginzburg Landau differential equation

$$\frac{\hbar^2}{4m} \left[\frac{\nabla}{i} - \frac{2e}{c} \mathbf{A} \right]^2 \psi(\mathbf{r}) = \epsilon_{nucl} \psi(\mathbf{r}) \quad (1)$$

which fulfills the given boundary conditions on the order parameter $\psi(\mathbf{r})$.

This approach is valid when we can neglect spatial variations of $|\psi(\mathbf{r})|$, such as thin films or wires of thickness $\ll \xi$ or when the applied magnetic field reduces $|\psi(\mathbf{r})|$ to a value much smaller than the equilibrium amplitude $|\psi_\infty|$ achieved deep inside the bulk superconductor. The regime of validity is then usually restricted to temperatures close to T_{co} .

An alternate approach is to extract ϵ_{nucl} at a given field from the measured $T_c^*(H)$ using the relation ^{11,12},

$$\ln \left[\frac{T_c^*}{T_{co}} \right] = \Psi \left[\frac{1}{2} \right] - \Psi \left[\frac{1}{2} + \frac{\epsilon_{nucl}}{4\pi k_B T_c^*} \right] \quad (2)$$

where $\Psi(x) = \Gamma'(x)/\Gamma(x)$ is the digamma function.

This relation describes the depression of $T_c^*(H)$ relative to T_{co} due to a magnetic perturbation. Though it was initially established by Abrikosov and Gor'kov for magnetic impurities ¹¹, further work by Maki ¹³ and de Gennes ¹² showed that it can be generalized to all pair breaking perturbations which destroy the time reversal symmetry of Cooper pairs. The scattering of the pair electrons should be rapid enough so that their relative phases can be randomized by the perturbation.

It can thus be applied to a dirty superconductor in strong external magnetic fields and only surrounded by insulators, if the mean free path l_{el} is much smaller than all sample dimensions and ξ_o or in the case of a small superconducting particle with all dimensions $\ll \xi_o$. Because the external field does not penetrate a bulk superconductor the sample thickness should be smaller than ξ and the penetration depth. In this case, ϵ_{nucl} corresponds to the energy difference acquired between time reversed electrons due to the magnetic field. At temperatures of the order of $T_c^*(H)$ it is sufficient to break the Cooper pair thus destroying superconductivity. When $T_c^* = 0$, (or $H = H_{c3}^*(0)$), ϵ_{nucl} coincides with the BCS superconducting gap $1.76k_B T_{co}$. Close to T_{co} the digamma function can be expanded around 1/2 and the $T_c^*(H)$ depression is linear in ϵ_{nucl} , $T_{co} - T_c^*(H) = \epsilon_{nucl}\pi/8k_B$.

The advantage of using Eq. 2 on the determination of ϵ_{nucl} is that it remains valid down to all temperatures. The linear Ginzburg-Landau results can be recovered if the temperature dependent coherence length is defined as $\xi^2(T) = D\hbar/\epsilon_{nucl}$, where $D = 1/3v_F l_{el}$ is the coefficient for electronic diffusion. For sample A, $D = 180\text{cm}^2\text{s}^{-1}$ obtained from the mean free path $l_{el} = 26.5\text{nm}$. Using $\xi^2(0) = \hbar D / 1.76k_B T_{co}$ we estimate $\xi(0) = 250\text{nm}$.

We calculated $\epsilon_{nucl}(H)$ for arrays A and B using Eq. 2 and the experimental T_c^* at the given applied field H.

In Fig. 2 we represent the results $\epsilon_{nucl}(H)$ normalized by the nucleation energy of a bulk superconductor, $\epsilon_{c2} = hDH/\Phi_o$ with the same coherence length as the array. The magnetic field is represented in reduced units

$HS_{hole}/\Phi_o = \Phi_{hole}/\Phi_o$, where S_{hole} is the hole surface. For comparison, we also represent the theoretical calculation for a circular hole on an infinite film (solid line) ¹⁴.

The representation $\epsilon_{nucl}/\epsilon_{c2}$ is equivalent to the inverse ratio of the nucleation fields H_{c2}/H_{c3}^* which close to T_{co} acquires the Ginzburg Landau form $H_{c2}/H_{c3}^* = (1 - T_c^*/T_{co}) H_{c2}(0)/H$ with $H_{c2}(0) = \Phi_o/2\pi\xi^2(0)$ using the coherence length as defined above.

On Fig. 2 we can observe that in the high field regime both samples are very well described by the theoretical calculation for a single hole. With decreasing fields the deviation from the single hole description is quite evident, with the appearance of the large period field modulations of one Φ_o per array cell and upward concavity. However we find a striking difference between both samples. The reduced energies $\epsilon_{nucl}/\epsilon_{c2}$ for sample B and for the single hole tend to an overall increase with decreasing field, reaching 1 at zero field. In contrast, for sample A, $\epsilon_{nucl}/\epsilon_{c2}$ decrease with decreasing field, dropping well below the single hole line. The studied samples have similar aspect ratios w/a , 0.54 (array A) and 0.53 (array B), respectively and similar ratios of the superconducting volume over the array cell volume V_s/V_{cell} , 0.79 (array A) and 0.82 (array B). We thus believe the distinct low field behavior is associated to the different ratio $w/\xi(T_c^*)$ between arrays, which close to T_{co} controls the process of edge nucleation and the type of coupling. Another interesting fact is that for both samples the last collective oscillation occurs for $w/\xi(T_c^*) \approx 3$.

On the following subsections we shall analyze the arrays distinct behavior by describing the array nucleation energy as coming from two main contributions: the nucleation energy of the single edge state and the coupling energy between neighbor edge states.

3.2. Wire networks of wide strands

As stated previously, sample A is well described by the single hole nucleation at high fields.

We shall thus focus on the behavior at low fields and consider the array energy as a sum of two contributions, the nucleation energy on the wires in parallel field $\epsilon_{strip\parallel}$ and a coupling energy. The coupling energy can be described within the framework of superconducting wire networks theory ^{4,5}. The case of superconducting wire networks of narrow wires is well understood. It can be treated as a periodic array of superconducting islands strongly coupled to the neighbor islands by thin superconducting wires of length a ($\xi \gg a$) and wire width $w \ll \xi$. Neglecting superconducting

fluctuations, the nucleation energy can be computed within mean-field theory by solving the linearized Ginzburg-Landau equations at each node of the network.

For a regular lattice (same length of all strands) the order parameter ψ_i on each site i will be coupled to the first neighbor sites through field dependent phase factors as,

$$4 \cos u \psi_i = \sum_j \psi_j \exp(-i\gamma_{ij}) \quad (3)$$

where 4 is the lattice coordination, $\gamma_{ij} = 2\pi/\Phi_o \int_i^j \mathbf{A} \cdot d\mathbf{l}$ is the phase factor along the wire linking site i to a site j due to the vector potential \mathbf{A} , $u = a/\xi = a\sqrt{(\epsilon_{wnt}/\hbar D)}$ is the strand length in units of $\xi(T)$ and ϵ_{wnt} is the wire network coupling energy.

Eq. 3 is equivalent to a tight binding equation. The coupling energy $\epsilon_{wnt} = \hbar D u^2 / a^2$ is then related to the ground state Landau level energy ϵ_{tb} of the tight binding model in the same geometry through $\epsilon_{tb} = 4 \cos u$ ^{15,16}. Taking into account the finite wire thickness, a more complicate relation between ϵ_{tb} and u is obtained, $\epsilon_{tb} = 4 \cos u + 4 \tan(uw/2a) \sin u - uw/a$ ¹⁷. This result established for zero external field can still be applied at low fields while there are no vortices in the wires.

In the inset of Fig. 3 is represented the field dependence of ϵ_{wnt} for array A, as a function of magnetic flux per array elementary cell Φ_{cell} , for Φ_{cell}/Φ_o between 0 and 1. ϵ_{wnt} is obtained from ϵ_{nucl} (calculated using Eq. 2 and the experimental $T_c^*(H)$) after subtracting the parabolic contribution of edge nucleation in the wires, $\epsilon_{strip \parallel}$. Since we are close to T_{co} , the variation of $T_{co} - T_c^*(H)$ due to the coupling (after subtracting the linear dependence on H) corresponds to $\epsilon_{wnt}\pi/8k_B$.

The ϵ_{wnt} results obtained using the solutions of the tight binding equation for rational values of $\Phi_{cell}/\Phi_o = p/q$ with $q < 30$ and $p < q$ are also represented. The coupling energy obtained using the relation for $w = 0$ is smaller than the experimental data. However we find a very good agreement with the theoretical results which take into account the finite wire thickness.

Besides the fundamental dips at $\Phi_{cell}/\Phi_o = 0, 1$ and at $1/2$, additional dips can be identified at the rational values $\Phi_{cell}/\Phi_o = p/q$, for $q = 3, 4$ and 5 . This fine field structure is an indication of the interference of quantum states over cells of size $qa \times qa$. With increasing fields the fine field structure becomes less pronounced and only the fundamental dips subsist until $\Phi_{cell}/\Phi_o = 8$. At higher fields the single hole regime is recovered.

Another feature of the low field behavior is the small values of $\epsilon_{nucl}/\epsilon_{c2}$ at integers Φ_{cell}/Φ_o , which correspond to nucleation fields H_{c3}^*/H_{c2} much higher than for single hole nucleation. This fact is due to an edge nucleation

controlled by two boundary conditions imposed at the edges of adjacent holes. We can get some insight by comparing the field dependence of the ϵ_{nucl} envelope curve with the nucleation energy for a strip or slab in an external parallel field, $\epsilon_{strip \parallel}$.

The field dependence of $\epsilon_{strip \parallel}$ for a strip or slab of intermediate thickness w , is strongly dependent on $w/\xi(T_c^*)$. This problem as well as the supercurrents distribution and vortex patterns on a thin slab were treated previously^{8,18,19}. The main features are as follows. Below a critical thickness $w < 1.84 \xi(T_c^*)$ (thin wire limit) nucleation starts symmetrically at both surfaces and the maximum of the order parameter occurs at middle distance between them. In this limit $\epsilon_{strip \parallel} = H^2 w^2 (\pi h D / 6 \Phi_o^2)$. With increasing field, when $w > 1.84 \xi(T_c^*)$, $\epsilon_{strip \parallel}$ deviates from the parabolic field dependence as the order parameter solutions at each surface pull apart, their superposition giving rise to nodes along the middle plane of the wire and equidistant of $\Delta L \approx \Phi_o / H w (1 - 1.84 \xi)$. The vortex pattern becomes more complex at higher fields. When the interference of the surface solutions become negligible, compared to $k_B T_c^*$, the one boundary solution is recovered. $\epsilon_{strip \parallel}$ then approaches the surface sheath limit $0.59 h D H / \Phi_o$.

On Fig. 3 we represent the nucleation energy ϵ_{nucl} of array A as a function of applied field and $\epsilon_{strip \parallel}$ ⁸ for a wire of width w equal to the array strands width. We can identify several similitudes. On the single hole regime the main dependence of ϵ_{nucl} is linear on H such as the field dependence of $\epsilon_{strip \parallel}$ in the surface sheath limit, in agreement with the dominance of 1 - boundary nucleation at the edges of each individual hole. With decreasing field both deviate from the linear H dependence due to the emergence of interference between adjacent surfaces solutions. This deviation occurs near the field $H_1 = 0.65 mT$ which corresponds to the position of the first important dip of $\epsilon_{nucl}/\epsilon_{c2}$ at $\Phi_{cell}/\Phi_o = 5$ (see also Fig. 4.b) due to interaction between neighbor holes. Below a field $H_o \approx 2.75 \Phi_o / \pi w^2$ ($0.39 mT$) nucleation starts symmetrically in the strip⁸ and the order parameter is maximum at middle distance between adjacent edges. The occurrence of symmetric nucleation on a restricted field regime explains why the wire network coupling description is still valid for arrays of wide strands. Though the array strands do not correspond to ideal infinite wires, in the regime $H < H_o$, we expect the collective dips of ϵ_{nucl} to approach the parabolic envelope of $\epsilon_{strip \parallel}$, as observed in Fig. 3, since at integers values of Φ_{cell}/Φ_o the costs in coupling energy are minimum. These results thus indicate that the wire network coupling is closely related with the 2 - boundary nucleation process.

Since the crossover from 2 - boundary to 1 - boundary edge nucleation is associated to the appearance of interstitial nodes of the order parameter within the strands, we expect a broadening of the array resistive transition

with increasing H due to the presence of weakly bounded interstitial vortices.

In Fig. 4 is represented the field variation of the resistive transition width $\Delta T_c^*(H)$ of array A, obtained by subtracting the transition lines $T_c^*(H)$ measured for resistive criteria $0.6R_n$ and $0.03R_n$. For comparison, we also represent the field variation of the distance ΔL between nodes on a single wire, normalized by the array lattice parameter $a = 4\mu m$.

At fields $H_o \leq 0.39mT$ (region I, $\Phi_{cell}/\Phi_o \leq 3$) the transition width at integer values of Φ_{cell}/Φ_o is the same as in zero field. Since in this regime nucleation starts symmetrically at each side of the strands, there are no order parameter nodes within strands, only coreless vortices on holes. At intermediate values of Φ_{cell}/Φ_o phase fluctuations lead to a broadening of the transition followed by a sharp jump at integer values of Φ_{cell}/Φ_o . This jumps correspond to the increase of the enclosed flux per hole by Φ_o .

At fields $H_o < H < H_1$ (region II, $3 < \Phi_{cell}/\Phi_o < 5.4$), the first nodes of the order parameter are expected to appear within the strands with a separation ΔL that drops from infinity to values comparable to the array lattice parameter. The sharp jumps at integers Φ_{cell}/Φ_o disappear since the array is able to follow the increase of field by accommodating vortices at interstitial positions. In particular, at $\Phi_{cell}/\Phi_o = 4$ there is no sharp variation of ΔT_c^* which may indicate that some holes do not increase the enclosed flux by one. This observation is in agreement with Fig. 4.b) where the field dependence of $\epsilon_{nucl}/\epsilon_{c2}$ represented as a function of Φ_{cell}/Φ_o shows that $\epsilon_{nucl}/\epsilon_{c2}$ at $\Phi_{cell}/\Phi_o = 4$ is higher than the adjacent dips.

At $\Phi_{cell}/\Phi_o = 5$ every hole encloses $4\Phi_o$ and the interstitial node distance should be $\approx a$. Vortices should occupy positions at the array interstices forming a stable sublattice, which favors the decrease of $\epsilon_{nucl}/\epsilon_{c2}$.

In region III, the transition width broadens considerably due to the appearance of the weakly bounded interstitial vortices as the distance between them drops below a . This distance is further reduced with increasing field until the wave function solutions at each hole edge become independent.

We can see from Fig. 4.b) that at $\Phi_{cell} = 8\Phi_o$ the $\epsilon_{nucl}/\epsilon_{c2}$ field modulation inverts concavity once the single hole nucleation becomes dominant. If for Φ_{cell}/Φ_o between 5 and 8, the increasing flux occupies interstitial positions and the enclosed flux per hole remains equal to $4\Phi_o$, ϵ_{nucl} should meet the single hole curve at its 4th oscillation, in agreement with the results presented on Fig. 2.

3.3. Weak link array of edge states

We do not expect the description of a wire network of wide strands to hold if holes edges are pulled apart and/or shaped to circles. This is the case of sample B where the minimum inter-hole distance is $w = 4.74\mu m$ (\sim twice compared to array A). The field for symmetric nucleation is $H_o \approx 0.08mT$ for a stripe with the same thickness. However since the distance between hole edges is not constant (varying from 4.74 to $9\mu m$ around the hole perimeter) H_o should be further reduced. As a consequence the parabolic envelope of ϵ_{nucl} is not observed. The coupling between neighbor edge states is still present though. Fundamental dips of ϵ_{nucl} at integers values of $\Phi_{cell}/\Phi_o \leq 7$ are clearly observed although we find no fine field structure²⁰. At low field $\epsilon_{nucl}/\epsilon_{c2}$ is lower than the single hole calculation indicating that the energy contribution due to the overlap between edge states is important.

In the next sections we present a simple model which is able to capture the transition from the single hole to the collective behavior for array B. The application of this model is based on the assumption that in a narrow temperature region $T_{c2} < T < T_c^*$ the superconducting edge states are localized close to the hole boundaries and the system behaves like an array of weak links. The fast oscillations observed at low fields are then related to the collective behavior of the array. Since there is nonzero overlap between the wave functions of different edges, the energy should be higher than that of a single hole. One consequence is that the nucleation field H_{c3}^* is lower than that of a single hole, as it is observed in the experiments. The single hole behavior is naturally recovered at higher fields where the overlap between neighboring edges vanishes.

A Ginzburg-Landau approach is suitable to study the problem. For the single hole, an analytical solution is available due to the cylindrical symmetry of the problem²¹. A variational approach for the determination of the order parameter has been analyzed by Buzdin⁶. The agreement with the exact solution is good except at low fields where the variational approach predicts a region with zero flux through the hole which is not present in the exact solution. Buzdin's variational approach, however, has the great advantage of being applicable also in the many holes case where an analytical solution is impossible to obtain.

We proceed as follows. We first describe an improved variational ansatz for the single hole case by using a trial order parameter of three parameters. We then construct an effective Ginzburg-Landau free energy which takes into account, in an approximate way, the edge coupling and we determine the resulting nucleation energy.

3.4. Variational approach : single hole

In this section we introduce the new variational wave function for the evaluation of the nucleation energy in a superconducting film containing a hole. Following Buzdin ⁶, the Ginzburg-Landau free energy (\mathcal{F}_N is the free energy of the normal state) is given by

$$\mathcal{F} - \mathcal{F}_N = \frac{\hbar^2}{4m} \int d^2r \left[\left| \left(-i\nabla - \frac{2\pi}{\Phi_o} \mathbf{A} \right) \psi(\vec{r}) \right|^2 - \frac{1}{\xi^2} |\psi(\vec{r})|^2 \right] \quad (4)$$

The fourth order term has been ignored since we are interested in the phase boundary. The surface critical field can be determined with a variational procedure by determining the minimum of the functional

$$\mathcal{F} - \mathcal{F}_N = 0 \quad (5)$$

within the class of trial wave functions $\psi(\vec{r})$ which satisfy the proper boundary condition at the superconductor-insulator interface

$$\left[\frac{\partial \psi}{\partial \rho} \right]_{\rho=R} = 0 \quad (6)$$

where R is the radius of the hole. For a hole containing m flux quantum, the order parameter has the following form in cylindrical coordinates (ρ, ϕ, z) ,

$$\psi = \frac{1}{\sqrt{2\pi}} F(\rho) e^{im\phi}$$

It is possible to improve the result obtained by Buzdin ⁶ by using a three-parameters trial order parameter of the form

$$F(x) = \left[1 + \alpha(x - x_0)^\eta + \beta(x - x_0)^\zeta \right] \exp \left[-\frac{\gamma}{2}(x - x_0)^2 \right] \quad (7)$$

where α, β, γ are the variational parameters and the dimensionless quantities $x = \rho(eH/c\hbar)^{1/2}$, $x_0 = R(eH/c\hbar)^{1/2} = (\Phi_{hole}/\Phi_o)^{1/2}$ has been introduced.

For the case of a single hole an exact solution for the nucleation energy is expressed in terms of the eigenvalues of the Kummer's equation ^{21,22}. We compare our results (the best results have been obtained for $\eta = 2$ and $\zeta = 2.05$) with the exact calculation and with the one parameter trial function ⁶. This is shown in Fig. 5. The trial function $F(x)$ given by Eq. (7) has a maximum at $(x - x_0)^2 \sim (2 - \gamma/(\alpha + \beta))/\gamma$, a feature which is also present in the exact solution. This seems to improve considerably the accuracy of the variational approach ²³.

The result obtained by using Eq. (7) improves considerably the agreement with the exact solution. In particular the spurious $m = 0$ is shrunk to very low fields ($< 0.03\Phi_o$).

3.5. Variational approach : array of holes

We obtain an approximate expression of the nucleation energy for a regular array using the variational wave function introduced in the previous section and an appropriate Ginzburg-Landau free energy which takes into account the overlap between edge states of adjacent holes. The model is sketched in Fig. 6, we will consider an array of edges connected by weak links (dashed lines in the figure). The crossover between the single hole and the collective behavior stems from the interplay of flux quantization on each hole and frustration effects through the elementary array cell.

The GL free energy which we propose has the following form

$$\mathcal{F} - \mathcal{F}_N = \sum_i \mathcal{F}_i + \sum_{\langle i,j \rangle} \mathcal{F}_{ij} \quad (8)$$

where \mathcal{F}_i is the free energy defined in Eq. (4) and the subscript i identifies the hole in the array. \mathcal{F}_{ij} takes into account the overlap between the holes.

We choose a \mathcal{F}_{ij} of the following form

$$\mathcal{F}_{ij} = \frac{\hbar^2}{4ma^2} \int d^2r \left[\alpha_o |\psi_i(\vec{r}) - \psi_j(\vec{r})|^2 + (\alpha_1 + \alpha_2 \delta_{ij}) |\psi_i(\vec{r})| |\psi_j(\vec{r})| \right] \quad (9)$$

The effect of the external magnetic field will be included in Eq. 9 by means of a Peierls substitution. We assume that the overlap is restricted to a small area (see the dashed lines in Fig. 6) and that the hole array can be treated as a weak link array. The first term in Eq. 9 is modified as follows

$$|\psi_i - \psi_j|^2 \rightarrow |\psi_i|^2 + |\psi_j|^2 - 2|\psi_i||\psi_j| \cos(\phi_i - \phi_j - \pi m - A_{ij}) \quad (10)$$

where $A_{i,j} = (2\pi)/(\Phi_0) \int_i^j \mathbf{A} \cdot d\mathbf{l}$ is calculated along the path indicated by the dashed lines in Fig. 6 (we assumed that all the holes contain the same number m of flux quantum).

The terms in Eq. 9 can be understood considering that the order parameter in the array of holes can be given as $\psi = \sum_i \psi_i$. Substituting this expression in the GL free energy of Eq. 4, one generates the various terms given above. In general since the approach is phenomenological, the various contributions enter with different coefficients ($\alpha_o, \alpha_1, \alpha_2$). It is important to stress that the total wave function does *not* satisfy the proper boundary conditions around the holes because of the exponential tails of the edge states of the neighboring island. Therefore this approach breaks down at very small field when the overlap becomes too strong.

The agreement of the experiments with the single hole result in the high flux regime indicates that phase fluctuations do not drive the phase

transition. In this case we can approximate the phase dependent part of the free energy by its ground state energy

$$\epsilon(\Phi_{cell}/\Phi_o) = \frac{2}{zN} \sum_{\langle i,j \rangle} \langle \cos(\phi_i - \phi_j - \pi m - A_{ij}) \rangle_{GS}$$

where N is the number of holes in the array, z is the coordination number, Φ_{cell}/Φ_o is the magnetic flux per elementary cell of the array and $\langle \dots \rangle_{GS}$ means the ground state configuration of the phases ϕ_i .

Going over the same steps as Buzdin ⁶ the nucleation energy for an array of holes is obtained by minimizing the following functional over the trial function introduced in Eq. 7

$$\begin{aligned} \frac{\epsilon_{nucl}}{\epsilon_{c2}} &= \mathcal{I} \int_{x_0}^{\infty} \frac{dx}{x} \left[(m - x^2)^2 F^2(x) + x^2 [F'(x)]^2 + g \frac{R^2}{a^2} \frac{1}{4x_0^2} x^2 [F(x)]^2 \right] \\ &+ g_1 \frac{R^2}{a^2} \frac{1}{4x_0^2} [2 - g_2 \epsilon(\Phi_{cell}/\Phi_o)] \langle F(x_i) F(x_j) \rangle \end{aligned} \quad (11)$$

where the overlap integral

$$\langle F(x_i) F(x_j) \rangle = \mathcal{I} \int d\vec{x} F(\vec{x}) F(\vec{x} + \frac{\vec{w}}{x_0}) \quad (12)$$

the normalization

$$\mathcal{I}^{-1} = 2 \int_{x_0}^{\infty} dx x F^2(x)$$

has been introduced. The new parameters g, g_1, g_2 are easily expressed as a function of the α 's.

In Fig. 7 we present the results obtained for various values of the three parameters g, g_1 and g_2 . We can observe that the presence of the Josephson coupling increases the array nucleation energy, relatively to the isolated hole case, and introduces cusps of different concavity superimposed over the main single hole background at low flux when the coupling becomes stronger. These features were found in the experiment of Bezryadin *et al* ¹. At very low fields $\epsilon_{nucl}/\epsilon_{c2}$ rapidly increases, as also seen in the experiments. It may be explained by the fact the the wave functions extends over various lattice constants and therefore the system does not show any surface superconductivity. However this model breaks down at flux typically of the order of $0.15\Phi_{hole}$.

A word of caution is needed at this point. Although the main features of the crossover are found one should be aware that the model is still too simplified to aim at a quantitative comparison with the experiments. In particular the choice of the values of the constants g is not related to any

microscopic model which allow to justify the numerical parameters. It is, however, rewarding that most of the qualitative features are captured by our model. A further step might be to apply the techniques developed by Palacios *et al* ²⁴ to the present problem.

4. Conclusion

In conclusion, we tried to show how geometric parameters such as the inter-hole and the array lattice constant can influence the transition temperature of periodic superconducting arrays as a function of a magnetic field.

Some of these points were already addressed ¹ and reanalyzed here. We found a clear crossover from single to a coupled edge state regime with decreasing field on the studied samples. The behavior of $\epsilon_{nucl}/\epsilon_{c2}$ in the single edge regime is very similar and the arrays transition depend exclusively on the magnetic flux per hole area. We should however remark that a quantitative comparison of the energy ratios $\epsilon_{nucl}/\epsilon_{c2}$ between samples need some caution since they are extremely dependent on the estimation of $\xi()$ and small errors can lead to a shift of the $\epsilon_{nucl}/\epsilon_{c2}$ value.

The coupling established at low fields was found to be well described either as a superconducting wire network coupling (strong coupling) or as a weak link interaction, depending on the inter-hole distance w , the defect shape and the coherence length at $T_c^*(H)$ which controls the edge nucleation process.

The low field behaviour of the studied samples is representative of two distinct coupled systems: the superconducting wire network (strong coupling) and the weak link array. In both cases the coupling is mediated by the frustration introduced by the applied field over the array elementary cell. However there is a fundamental difference between the field dependence of the coupled edge states. In the case of the weak link array (array B) we have coupled single hole edge states which depend on H through the enclosed flux per hole. The array transition is then dominated by the single hole nucleation. As a consequence the flux per hole does not necessarily increase with the flux per cell since the increase of the hole winding number may be less favorable than placing flux at the array intertices where superconductivity is weakened.

In the case of the wire network system (array A at low fields), we have a coupling between the order parameter at the array nodes, which is determined by symmetric nucleation. In this case the array transition is dominated by thin wire nucleation and depends only on H , as seen on Fig.3. The flux enclosed per hole or per array cell are equivalent quantities as long as

interstitial vortices are not allowed within the array strands.

This explains why the studied samples who have similar geometric ratios ($w/a \approx 2$ and $V_s/V_{cell} \approx 0.8$) exhibit such a different collective behaviour at low fields. The relevant parameters are then the inter-hole distance (which allows 2 - boundary nucleation in a wide field regime for sample A) and the parallel hole edges which favour the thin wire nucleation.

Our results indicate these parameters are determinant for the low field collective behaviour. For periodic arrays of close enough defects ($w/\xi(T_c^*) < 1.84$) and parallel hole edges, the coupling between edge states can be described as a wire network coupling. In this case, the array transition approaches the thin wire nucleation limit at low fields. As a consequence the array transition are not necessarily upper (lower) bounded by the semi-infinite plane result $H_{c3}/H_{c2} = 1.69$ ($\epsilon_{nucl}/\epsilon_{c2} = 0.59$) or the single hole nucleation limit, showing higher nucleation fields.

In the limit where 2 - boundary nucleation does not occur due to a higher inter-hole distance (and/or hole shape) the wire network formalism is not suitable to describe edge states coupling since we can not neglect variations of the order parameter amplitude between holes. In this case the array transition is dominated by single hole edge states. We thus presented an alternative description based in a weak link interaction between single edge states which allows to recover the main features of the $T_c^*(H)$ line on the low field regime: the inversion of field modulation concavity and the presence of periodic upward cusps. In addition it reproduces the experimental observation that the array transition occurs at temperatures above the single edge nucleation, which is associated both to the dominance of the single hole nucleation and to the increase of the array energy due to the overlap between neighbor single edge wave functions.

5. Acknowledgments

We would like to thank G. Falci and O. Buisson for useful discussions. We acknowledge the financial support of the European Community (Contract FMRX-CT-97-0143). C.C. Abilio is supported by a grant PRAXIS XXI (5713/95) of the Portuguese Ministry for Science and Technology.

REFERENCES

1. A. Bezryadin, and B. Pannetier, *Physica Scripta* **T66**, 225 (1996); A. Bezryadin and B. Pannetier, *J. Low Temp. Phys.* **98**, 251 (1995).
2. A.T. Fiory, A.F. Hebard, and S. Somekh, *Appl. Phys. Lett.* **32**, 73 (1978).

3. M. Baert, V.V. Metlushko, R. Jonckheere, V.V. Moschalkov, and Y. Bruynseraede, Phys. Rev. Lett. **74**, 3269 (1995).
4. S. Alexander, Phys. Rev. B **27**, 1541 (1983).
5. R. Rammal, T.C. Lubensky, and G. Toulouse, Phys. Rev. B **27**, 2820 (1983).
6. A.I. Buzdin, Phys. Rev B **47**, 11416 (1993). Buzdin has chosen a trial form of $F(\rho)$ of the type $F(x) = \exp[-\frac{\gamma}{2}(x - x_0)^2]$
7. O. Buisson, P. Gandit, R. Rammal, J.C. Villegier, Phys. Rev. Lett. **53**, 1845 (1984).
8. D. Saint-James, and P.G. Gennes, Phys. Lett. **7**, 306 (1963).
9. L.G. Aslamazov and A.I. Larkin, Phys. Lett. **26A**, 11416 (1993).
10. W.A. Little and R. Parks, Phys. Rev. A **44**, 97 (1964).
11. A.A. Abrikosov, *Fundamentals of the theory of metals*, North-Holland (1988), Chap. 21.
12. P.G. de Gennes, *Superconductivity in Metals in Alloys*, (Benjamin, New York), 1966, Chap. 8.
13. K. Maki, *Superconductivity*, ed. R.D. Parks (Dekker, New York), 1969, ch.18.
14. A. Bezryadin, Yu.N. Ovchinnikov and B. Pannetier, Phys. Rev. B **53**, 8553 (1996).
15. D.F. Hofstadter, Phys. Rev. B **14**, 2239 (1976).
16. B. Pannetier, J. Chaussy, R. Rammal and J.C. Villegier, Phys. Rev. Lett. **53**, 1845 (1984).
17. Y.Y. Wang, B. Doucot, R. Rammal and B. Pannetier, Phys. Lett. A **199**, 145 (1986).
18. H.J. Fink, Phys. Rev. **177**, 1017 (1969).
19. H.A. Schultens, Z. Physik **232**, 430 (1970).
20. The absence of fine field structure could be interpreted as due to the presence of coherence only at a first neighbors level or due to the amplitude oscillations being smaller than our temperature resolution.
21. A. Bezryadin, A.I. Buzdin, and B. Pannetier, Phys. Rev. B **51**, 3718 (1995); Yu.N. Ovchinnikov, Sov. Phys. JETP **52**, 755 (1980).
22. R. Benoist and W. Zwerger, Z. Phys. B **103**, 377 (1997).
23. M. Tinkham, *Introduction to Superconductivity*, (Mac Graw-Hill New York, 1996).
24. J.J. Palacios, Phys. Rev. B **57**, 10873 (1998).

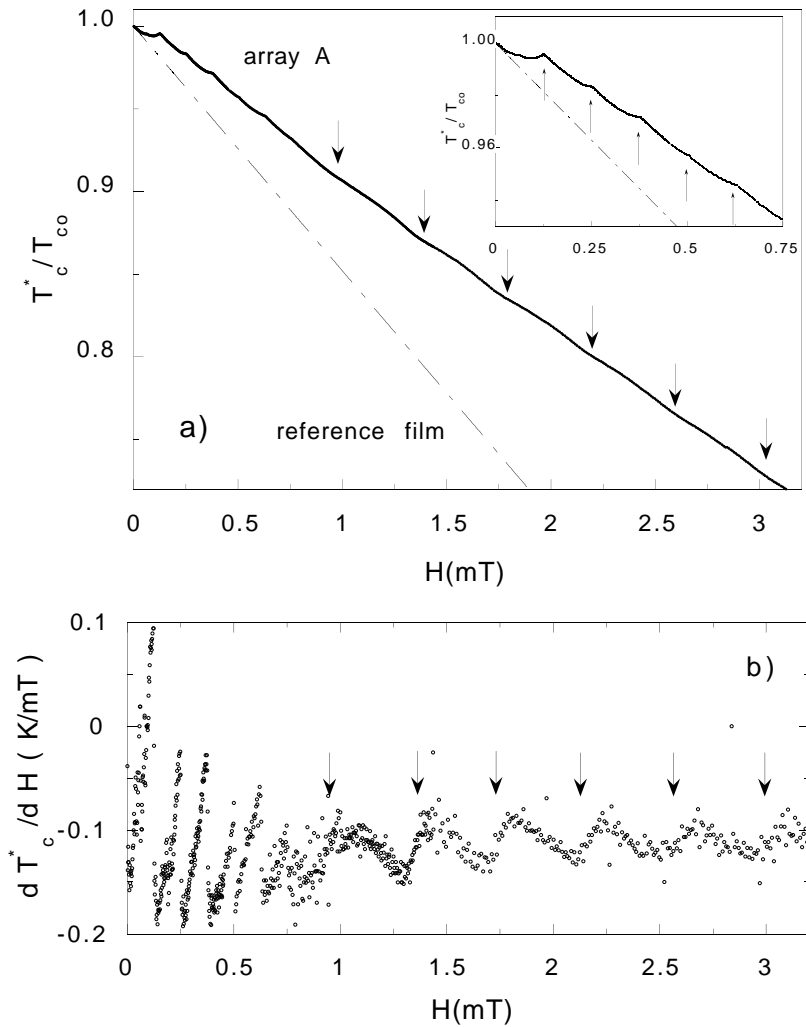


Fig. 1. a) Field dependence of the superconducting transition line $T_c^*(H)$ of array A (solid line) and of the reference sample $T_{c2}(H)$ (dashed line). Two types of field modulation are clearly identified for array A: downward, large period oscillations with dips at half integers of Φ_0 per hole (down arrows) and upward oscillations of shorter period with cusps at integers of Φ_0 per array elementary cell (inset:up arrows); b) $T_c^*(H)$ slope for array A as a function of H . The change of magnetic period due to the crossover from collective to single hole regime is quite visible.

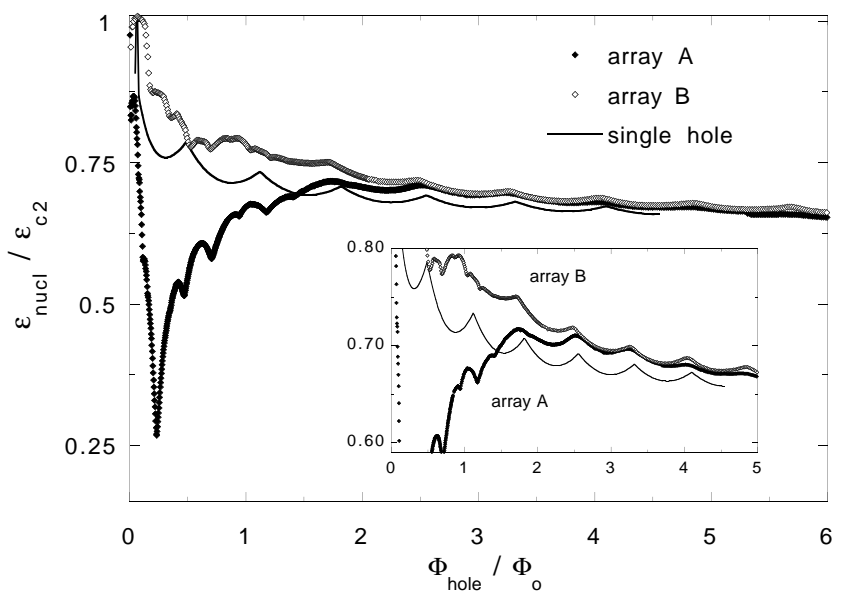


Fig. 2. Normalized nucleation energies $\epsilon_{nucl} / \epsilon_{c2}$ as a function of magnetic field (in units $HS_{hole}/\Phi_o = \Phi_{hole}/\Phi_o$), for sample A (solid dots), sample B (open diamonds) and the theoretical calculation for a cylindric cavity in an infinite thin film (solid line).

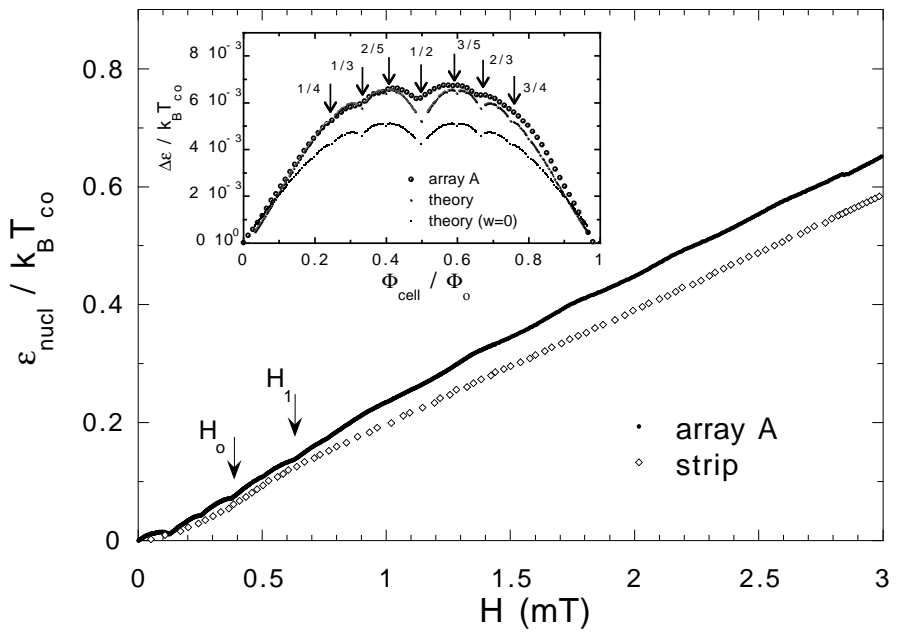


Fig. 3. Field dependence of the nucleation energies of array A (solid dots) and for a strip of width $w = 2.15\mu\text{m}$ (open diamonds), normalized by $k_B T_{\text{co}}$. In the field range $H_o < H < H_1$ interstitial vortices appear within strands. Inset: Coupling energy ϵ_{wnt} for array A (solid dots) and the theoretical ϵ_{wnt} for a superconducting wire network with $w = 0$ (small dots; lowest curve) and taking into account the wire thickness (small dots, upper curve) as a function of reduced field $\Phi_{\text{cell}} / \Phi_o$ between 0 and 1. The main dips position at rationals p/q ($q=3,4,5$) are indicated by down arrows.

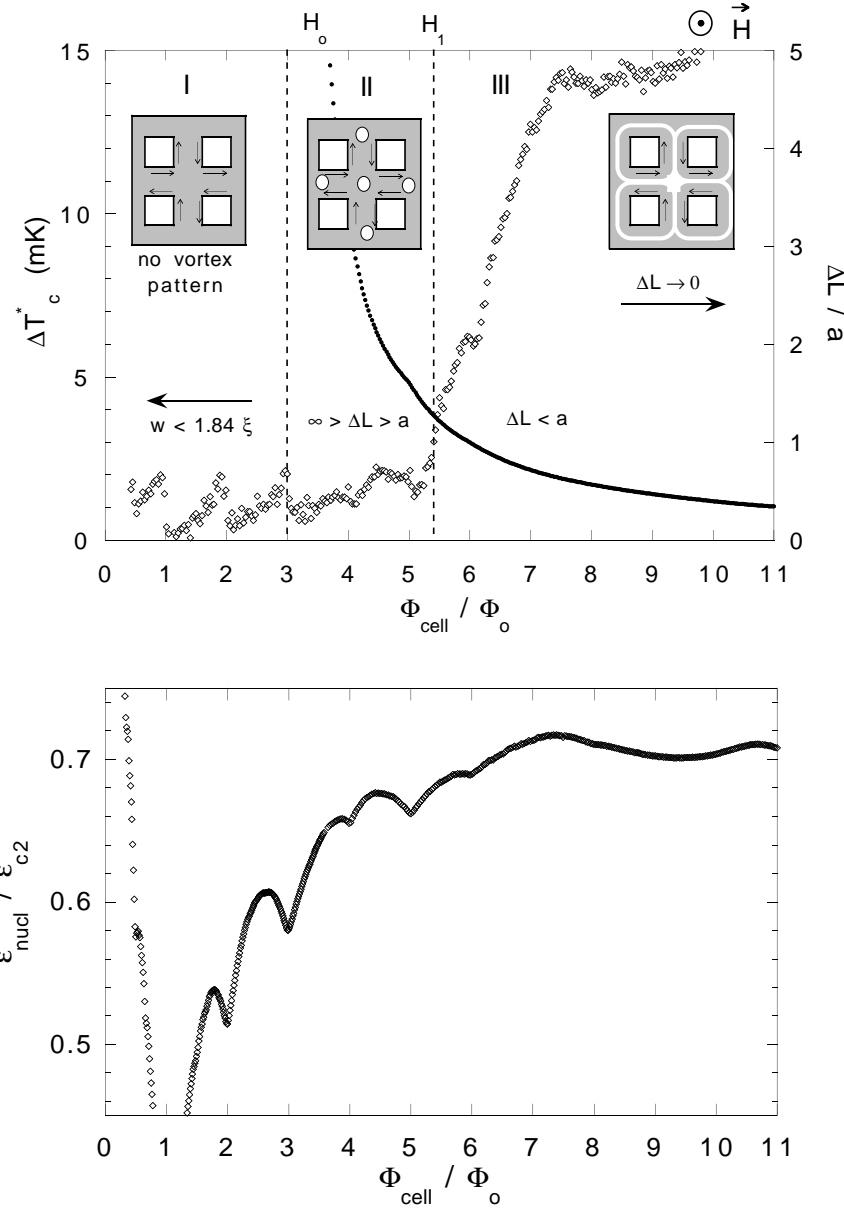


Fig. 4. a) Resistive transition width ΔT_c^* of array A (open diamonds) as a function of the reduced flux, $\Phi_{\text{cell}}/\Phi_o$ and comparison with the normalized distance $\Delta L/a$ between interstitial vortices for a thin wire (solid dots). An oversimplified picture of the vortex patterns developed within the wires is represented. Three main regions can be identified: (I) $w < 1.84\xi(T)$, nucleation starts symmetrically and there is no vortex in the wires; (II) $w > 1.84\xi(T)$ and $\infty > \Delta L/a \leq 1$, nodes of the order parameter appear at interstices due to the interference of neighbor edge wave functions (white dots); (III) $\Delta L/a < 1$ and decreases with increasing field until the surface solutions become independent and the single edge states are localized around each hole. b) field variation of the nucleation energy $\epsilon_{\text{nucl}}/\epsilon_{c2}$ for array A.

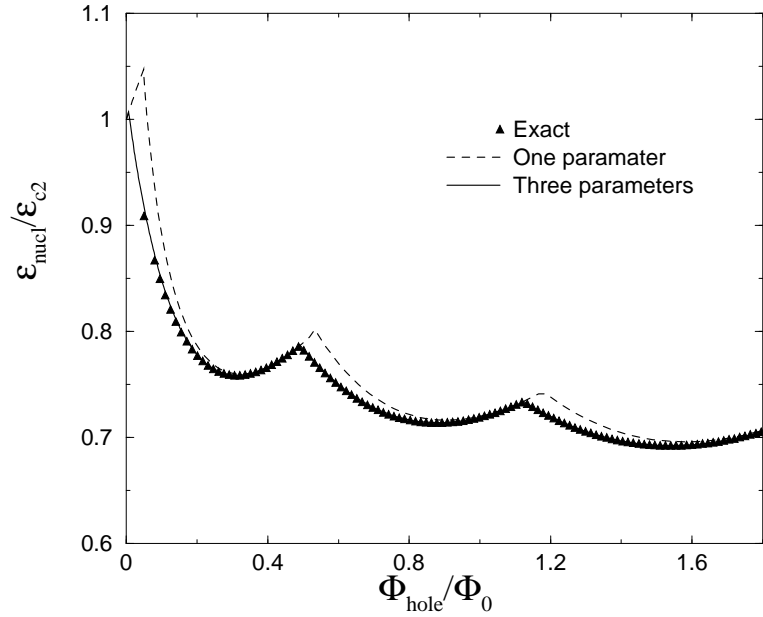


Fig. 5. Variational approximations for $\epsilon_{\text{nuc}}/\epsilon_{c2}$. The thick curve is obtained using the three parameter variational wave function. For comparison the curve obtained from the one parameter variational function is reported (dashed line).

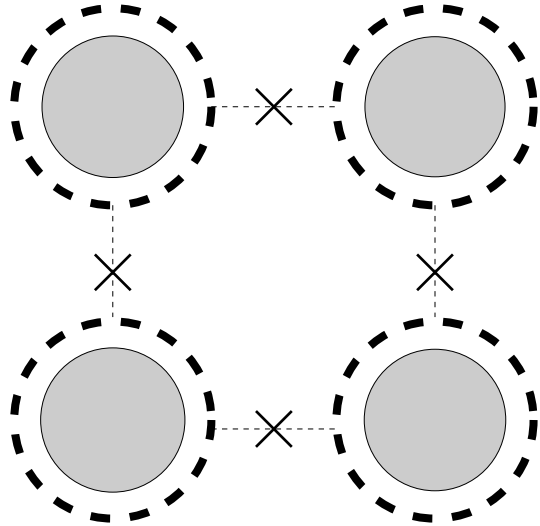


Fig. 6. Hole array. The dark regions represent superconducting surface sheaths due to localization of the edge states around each hole. The dashed lines mimic the coupling between adjacent edge states.

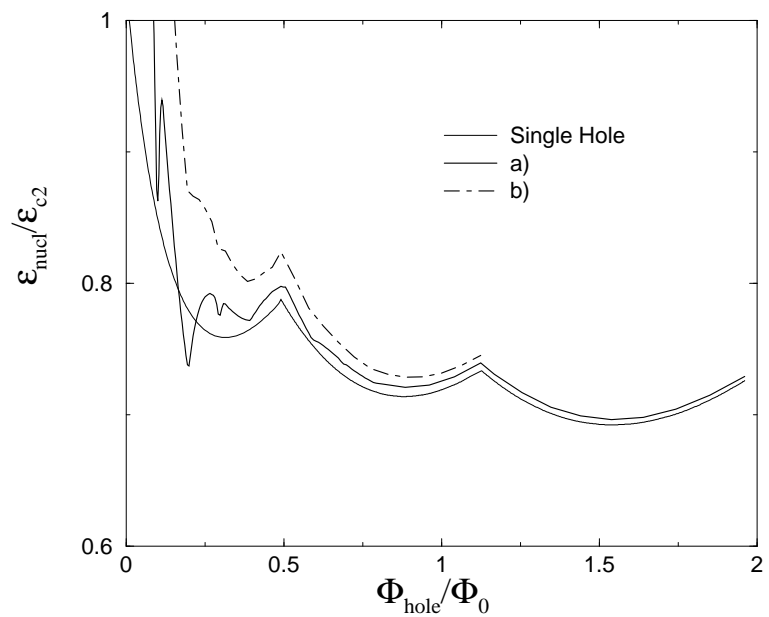


Fig. 7. The normalized nucleation energy $\epsilon_{nucl}/\epsilon_{c2}$ for a regular array of holes obtained by minimizing the functional as defined in the text for various parameter values. a) $g=0.1$ $g1=0.4$ $g2=1.6$; b) $g=0.2$ $g1=0.7$ $g2=0.9$.